

Performance and Stability of Organic Solar Cells Bearing Nitrogen Containing Electron Extraction Layers

Rico Meitzner,* Juliette Essomba, Shahidul Alam, Aman Anand, Nora Engel, Kevin Fulbert, Krisna Kuma, Fernanda Ayuyasmin, Md Moidul Islam, Chikezie Ugokwe, Ulrich S. Schubert, and Harald Hoppe*

Charge extraction and transport layers represent an important component of organic solar cells. Many different material groups are reported for these layers. Two important classes are metal oxides and organic materials. Many of these organic materials which are used as electron extraction layers (EELs) are nitrogen containing. Therefore, it has been decided to study a broad array of—to the largest part so far not reported—amine and imine containing organic materials as EELs in organic solar cells and compare them with an archetypical metal oxide electron transport layer (ETL). It enables certain structure–property relationships to be obtained for the EELs and to understand what determines their performance to a large part. Furthermore, their effect on the stability of organic solar cells is studied and they are found to be reasonable replacements as a cheap, quickly processable, environmentally friendly, biocompatible, and biodegradable alternative as compared with ETLs.

1. Introduction

Organic solar cells (OSCs) are a promising solar energy conversion technology, due to their potential for fast processing via roll-to-roll manufacture, their usage of earth abundant materials, their small environmental footprint, and last but not least their flexibility and general freedom in design. By today there are already several examples of notably high performances because the power conversion efficiencies of OSCs surpassed 15% since the year 2019.^[1] The most commonly used design today for solution-processed

OSCs is the bulk-heterojunction,^[2] where an active layer, which is a blend of an organic semiconductor acting as donor and one acting as acceptor, is sandwiched between two charge transport (CTL) or charge extraction layers (CEL), which themselves are adjacent to electrodes, whereby one of these electrodes has to be transparent.

These CELs have a strong impact on both performance and stability of OSCs.^[3] They, thereby, have to possess an array of qualities such as high transparency, easy processability, a suitable work function (WF)/energy levels, high abundance, and a low price.^[3e] There are many different classes of CTLs/CELs; these include metal oxides, inorganic and organic semiconductors, organic molecules with high dipole moments, and hybrids of the aforementioned categories.^[3e]

From the standpoint of solution processability and high abundance, organic CTLs/CELs are in particular interesting and have been extensively studied.^[3c,e,4] Two well-known organic polymers used as electron extraction layer (EEL) in organic solar cells are poly(ethylene imine) (PEI) and ethoxylated poly(ethylene imine) (PEIE).^[4a,e,5] Both of these polymers are insulators and are used to modify the WF of the adjacent electrode through their large dipole moment.^[4a] It was shown that they do so in inverted OSCs by chemisorption to substrates such as indium tin oxide or zinc oxide and, thereby, align their dipole moment properly to


R. Meitzner, J. Essomba, Dr. S. Alam, A. Anand, K. Fulbert, K. Kuma, F. Ayuyasmin, M. M. Islam, C. Ugokwe, Prof. U. S. Schubert, Dr. H. Hoppe
Center for Energy and Environmental Engineering (CEEC Jena)
Friedrich Schiller University Jena
Philosophenweg 7a, 07743 Jena, Germany
E-mail: rico.meitzner@uni-jena.de; harald.hoppe@uni-jena.de

R. Meitzner, J. Essomba, Dr. S. Alam, A. Anand, N. Engel, K. Fulbert, K. Kuma, F. Ayuyasmin, M. M. Islam, C. Ugokwe, Prof. U. S. Schubert, Dr. H. Hoppe
Laboratory for Organic and Macromolecular Chemistry (IOMC)
Friedrich Schiller University Jena
Humboldtstrasse 10, 07743 Jena, Germany

N. Engel, Prof. U. S. Schubert
Jena Center for Soft Matter
Friedrich Schiller University Jena
Philosophenweg 7, 07743 Jena, Germany

K. Fulbert, K. Kuma, F. Ayuyasmin
Faculty of Industrial Engineering
Ernst-Abbe-Hochschule Jena
07745 Jena, Germany

K. Fulbert, K. Kuma, F. Ayuyasmin
Faculty of Life Sciences and Technology
Swiss German University
15143 Banten, Indonesia

 The ORCID identification number(s) for the author(s) of this article can be found under <https://doi.org/10.1002/ente.202000117>.

© 2020 The Authors. Published by Wiley-VCH GmbH. This is an open access article under the terms of the Creative Commons Attribution License, which permits use, distribution and reproduction in any medium, provided the original work is properly cited.

Correction added on 6 January 2021, after first online publication: Rico Meitzner was designated as corresponding author.

DOI: 10.1002/ente.202000117

adjust the WF of the electrode to enable an improved contact and efficient charge carrier extraction.^[4a]

Recently, α -poly-L-lysine^[4c] was reported as an efficient EEL in conjunction with different active layer blends, fullerene- and nonfullerene-based alike. In this study, the materials derived from an amino acid outperformed other organic electron transport materials such as PDINO (3,3'-(1,3,8,10-tetraoxo-1,3,8,10-tetrahydroantra[2,1,9-def:6,5,10-d'e'f']diisoquinoline-2,9-diyl) bis(*N,N*-dimethylpropan-1-amine oxide)), PFN (poly[(9,9-bis(3'-(*N,N*-dimethylamino)propyl)-2,7-fluorene)-*alt*-2,7-(9,9-dioctylfluorene)]), and PFN-Br (poly[(9,9-bis(3'-(*N,N*-dimethyl)-*N*-ethylammonium)-propyl)-2,7-fluorene)-*alt*-2,7-(9,9-dioctylfluorene)]). Also, the amino acid serine^[6] was reported as an EEL and resulted in a good performance. More recently, the use of a simple amino acid (glycine) for modification of the EEL ZnO has been demonstrated. Indeed, the WF shifted slightly upward ($-4.11 \rightarrow -4.02$ eV), improving the performance.^[7]

On the contrary, such amine/imine compounds are also able to improve the contact by reducing surface recombination at the interface between active layer and electrode. Between organic semiconductors and reactive metals like aluminum, interfacial states can be formed; these states can help to form an ohmic contact between the semiconductor and the metal.^[8] These interfacial states can result in injection of charge carriers from the electrode into the organic semiconductor; this can limit the achievable fill factor of such devices.^[9] Also, surface recombination has a pronounced impact on the open-circuit voltage.^[10] For nonconducting materials such as poly(methyl methacrylate) (PMMA), Hu et al. reported no change in WF upon metal deposition, which they interpreted as no interaction between metal and polymer, but for polymers such as polyethylene oxide (PEO) and polyvinylpyrrolidone (PVP) they observed a change in WF, which they explained with coordinative interactions between these polymers and the electrode.^[11] Kim et al.^[12] described several strategies used in the field of perovskite solar cells used to passivate defect states based on the Lewis basicity of materials, for example, nitrogen atoms in pyridine were used to passivate defects. They also described the usage of PVP for both

defect passivation and reduction of interfacial recombination due to the Lewis base nature of PVP.^[12]

Another important factor is the stability of devices built with such interfacial layers. Courtright et al.^[5d] used PEI with different molar masses as part of a double-layer ETL in conjunction with ZnO and obtained a stability improvement over only ZnO, which was dependent on the molar mass of the PEI and improved with the same. Kim et al.^[5a] reported the stability of inverted OSCs containing PEIE as the sole EEL and retained above 80% of the initial performance after 30 days of storage under ambient conditions. This indicates potential for nitrogen containing organic materials as efficient electrode modifiers for organic solar cells.

We investigated several amine and/or imine containing organic molecules and polymers in CELs, to learn about structure–property relations. The organic compounds used as EELs and the layer stack used for all devices used for the experiments are shown in **Figure 1**. Furthermore, we investigated the stability of solar cells processed with the same and compared this with our reference material for the ETL, which is sol–gel-processed TiO_x .^[13]

2. Results and Discussion

First, a layer thickness optimization for the EELs was performed. The results of this optimization are shown in Figure S1, Supporting Information. Some of the materials showed only a weak dependence on the spin frequency, such as L-lysine and L-arginine, which may indicate low film thickness in general. However, others revealed a strong dependence such as L-histidine and especially the amine-rich polyoxazoline copolymer. The highest performance could be achieved with L-arginine, even in comparison with various differently processed TiO_x layers, as shown in **Table 1**. Due to the relatively large device area of 0.42 cm^2 , the devices showed in general a performance distribution at the intermediate range of the values reported for this material system.^[14]

The devices with L-arginine as EEL showed an open-circuit voltage which got closest to the maximum reported for this

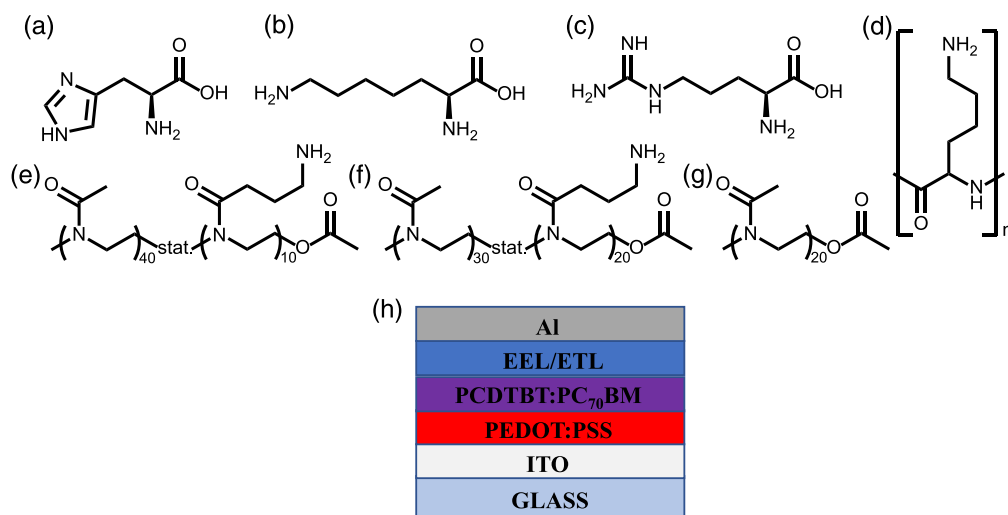


Figure 1. Schematic representation of organic materials used as EELs: a) L-histidine, b) L-lysine, c) L-arginine, d) poly-L-lysine, e) $\text{P}(\text{MeOx}_{40}\text{-stat-AmOx}_{10})$, f) $\text{P}(\text{MeOx}_{30}\text{-stat-AmOx}_{20})$ and g) PMeOx_{20} . h) The active layer stack used for the devices used for the experiments, which was a conventional layer stack.

Table 1. Photovoltaic parameters of the solar cells with different layer stacks. All values are averages with the respective standard deviation.

EEL	V_{OC} [mV]	J_{SC} [mA cm^{-2}]	FF [%]	PCE [%]	R_S [Ω]	R_{Sh} [$\text{k}\Omega$]
L-Histidine	832 ± 19	11.12 ± 0.33	48.3 ± 0.5	4.46 ± 0.23	16.0 ± 1.8	1.05 ± 0.06
L-Lysine	858 ± 12	11.27 ± 0.15	49.0 ± 0.8	4.73 ± 0.09	15.3 ± 3.2	0.90 ± 0.25
L-Arginine	869 ± 7	10.99 ± 0.34	51.3 ± 1.0	4.89 ± 0.12	12.0 ± 0.0	1.30 ± 0.09
Poly-L-lysine	850 ± 22	11.06 ± 0.37	49.8 ± 1.7	4.68 ± 0.42	13.3 ± 1.5	1.26 ± 0.06
P(MeOx ₄₀ -stat-AmOx ₁₀)	857 ± 9	10.11 ± 0.20	46.5 ± 2.4	4.02 ± 0.17	13.8 ± 1.5	0.98 ± 0.13
P(MeOx ₃₀ -stat-AmOx ₂₀)	854 ± 18	10.65 ± 0.50	50.0 ± 0.0	4.55 ± 0.26	14.0 ± 3.6	1.22 ± 0.06
PMeOx ₂₀	795 ± 16	10.20 ± 0.12	44.8 ± 0.5	3.62 ± 0.03	16.3 ± 1.3	0.92 ± 0.05
No EEL	656 ± 18	10.53 ± 0.24	43.8 ± 0.5	2.94 ± 0.16	184.5 ± 72.9	0.68 ± 0.03
Methanol overcast on PAL (no EEL)	772 ± 9	10.80 ± 0.20	45.8 ± 0.5	3.81 ± 0.14	10.3 ± 0.5	0.98 ± 0.05
TiO _x reference	670 ± 315	9.75 ± 0.73	41.0 ± 10.7	3.00 ± 1.77	11.3 ± 1.0	0.69 ± 0.49
TiO _x diluted	842 ± 5	9.14 ± 0.08	44.5 ± 1.0	3.45 ± 0.07	17.5 ± 1.3	0.97 ± 0.05
TiO _x unannealed	784 ± 12	10.45 ± 0.26	47.8 ± 1.3	3.92 ± 0.13	9.8 ± 1.0	1.04 ± 0.08

system, which is around 900 mV for all of the devices.^[15] The short-circuit current density of most devices was between 10 and 11 mA cm^{-2} , which is close to the maximum for this system, which is around 12 mA cm^{-2} . Only if devices were processed with TiO_x photocurrent densities were lower, which might be due to induced aggregation of the PC₇₁BM.^[16] The fill factor of the L-arginine-based device reaches above 50% and the overall performance of these devices is close to 5%, which is a good performance for this photoactive layer (PAL). The series resistance is close to 10 Ω , which is a decent result for devices with an area of 0.42 cm^2 , whereas the shunt resistance is clearly above 1 $\text{k}\Omega$, which is a good result for an organic solar cell.

While the device without any EEL showed a pronounced S-shape—corresponding to a blocking contact—at the open-circuit voltage (V_{OC}),^[17] a simple overcast with methanol *via* solvent dripping and spin casting resulted in an ohmic contact and an improved performance.^[18] The *I*-*V* curves of these devices are shown in Figure 2.

Devices with polyoxazoline polymers as ETL show an improving performance with increasing amine content with respect to

the amine groups in the side chain (with PMeOx₂₀ having 0% content, P(MeOx₄₀-stat-AmOx₁₀) having 20% amine content, and P(MeOx₃₀-stat-AmOx₂₀) having 40% amine content). The correlations between amine content and the photovoltaic parameters are shown in Figure 3. All photovoltaic parameters are roughly improved by about 10% for increased amine content, leading to a performance improvement by one-third. This is accompanied by a 40% drop in the series resistance and an increase by nearly 40% of the parallel resistance, demonstrating the effect coming from the CEL and its impact on selectivity and ease of charge extraction. Indeed, a further increase in the amine content does promise even higher performance parameters because no saturation was visible so far.

It was especially attractive that the amino acids performed so well, as they are low cost and show no issue with reproducibility, unlike polymers, which can vary from batch to batch. We investigated more in depth in how far the structural differences between the amino acids affected their performance. It is well established that the dipole moment of nitrogen containing organic molecules impacts performance in organic solar cells.^[4a]

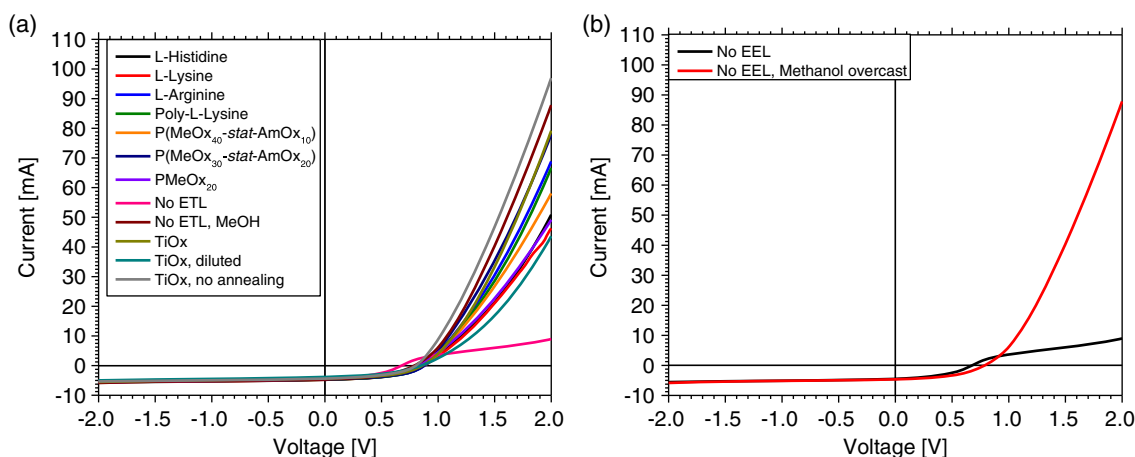


Figure 2. a) *I*-*V* curves for all solar cells before degradation and b) specifically again for the devices without EEL. The device without methanol overcast shows a severe S-shape around the open-circuit voltage, while that S-shape is entirely suppressed for the device with the methanol being overcast on the active layer before electrode deposition.

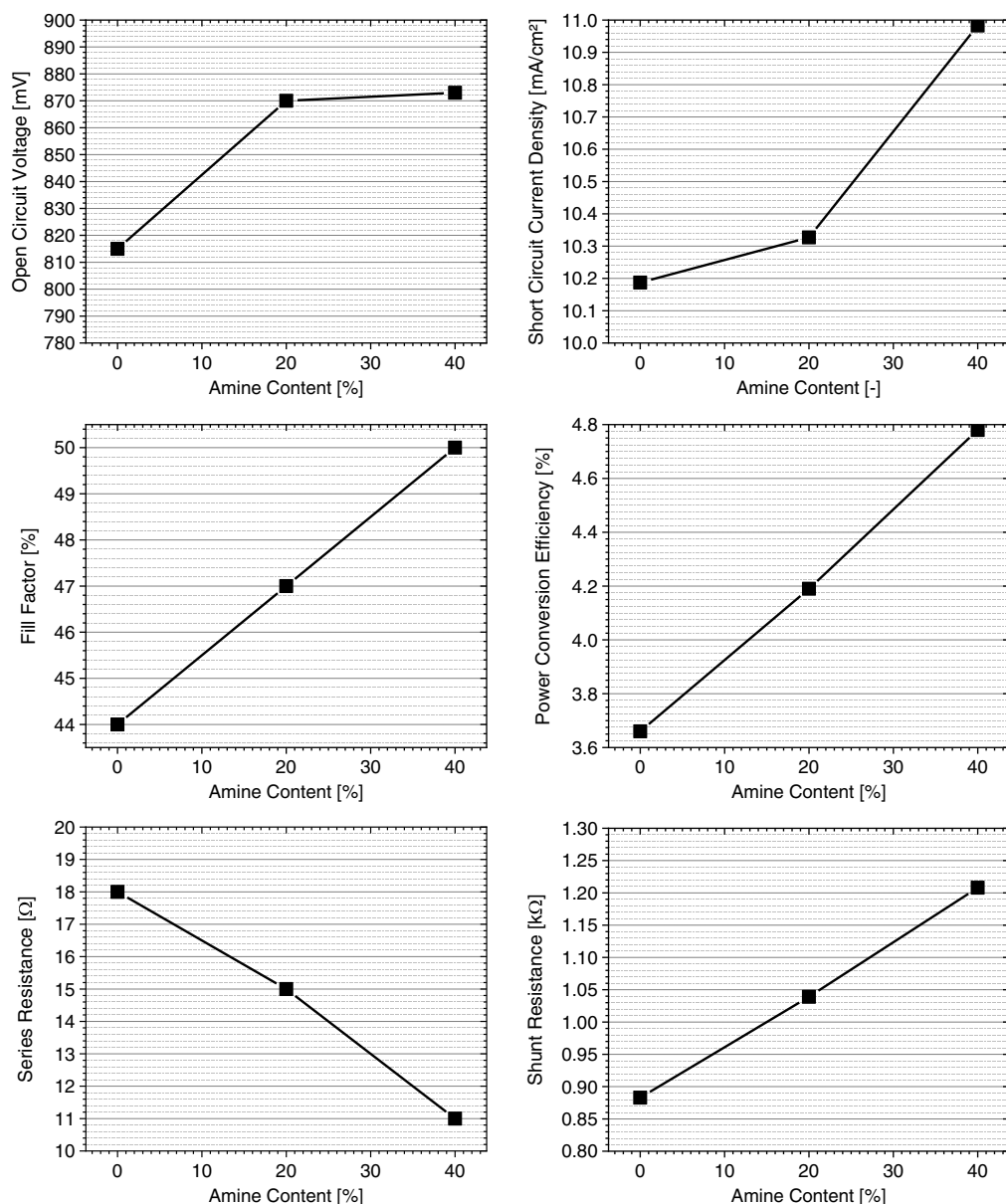


Figure 3. Correlations between amine content in the polyoxazoline polymer and statistical copolymers with the photovoltaic parameters of the solar cells containing the respective polymers as EEL.

All of the polar groups in these amino acids are proton donors or proton acceptors. Therefore, special attention was paid to the dissociation constants of the amine/imine and carboxylic groups within the amino acids.

In **Figure 4**, the correlation between dissociation constants of the different polar groups with respect to their position in the molecule and open-circuit voltage, fill factor, power conversion efficiency, and series resistance is shown. Figure 4a shows a clear direct proportionality between the dissociation constant of the amine/imine group in the side chain and the open-circuit voltage; the same is observed in Figure 4b,c for fill factor and power conversion efficiency. However, Figure 4d shows an inverse proportionality between dissociation constant and series resistance.

The dissociation constant of the different amine/imine groups is a direct proxy for the polarity of the respective groups, i.e., how willingly the nitrogen of the amine group will share its nonbinding electron pair and, therefore potentially, for their dipole moment. This correlation can be understood, if the amino acids are forming a mostly ordered layer on top of the active layer with the dipole moment of the amine/imine group in the side chain facing toward the active layer, which was reported in the past for PEI and PEIE by Zhou et al.^[4a]

To yield a better understanding for the effect of the EELs, Kelvin probe measurements were performed on samples consisting of layer stacks as sketched in the inset of **Figure 5b**. These measurements have been performed either in the dark or in under illumination, with a corresponding excitation density of

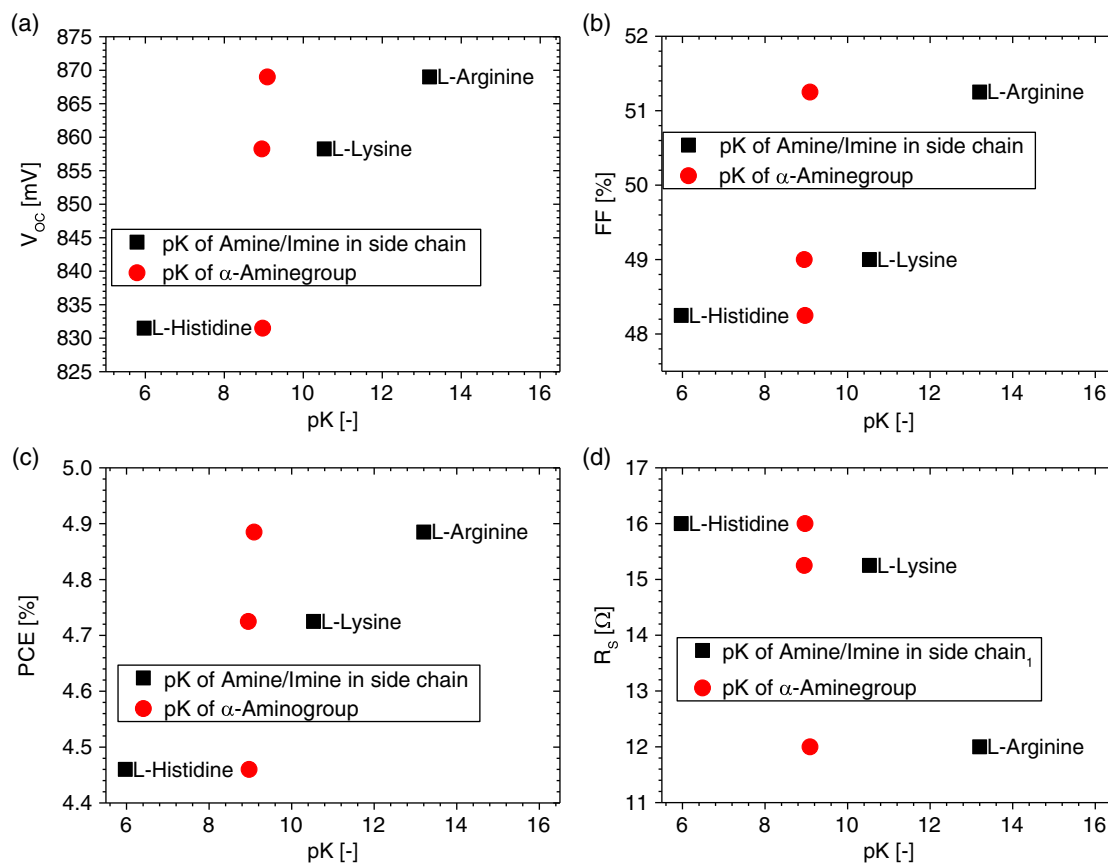


Figure 4. a) Dependence of the open-circuit voltage, b) fill factor, c) PCE, and d) R_s on the dissociation constant of the amine/imine group in side chain and α -amine group. There is a clear increase in V_{OC} with increasing pK of the side chain amine/imine group.

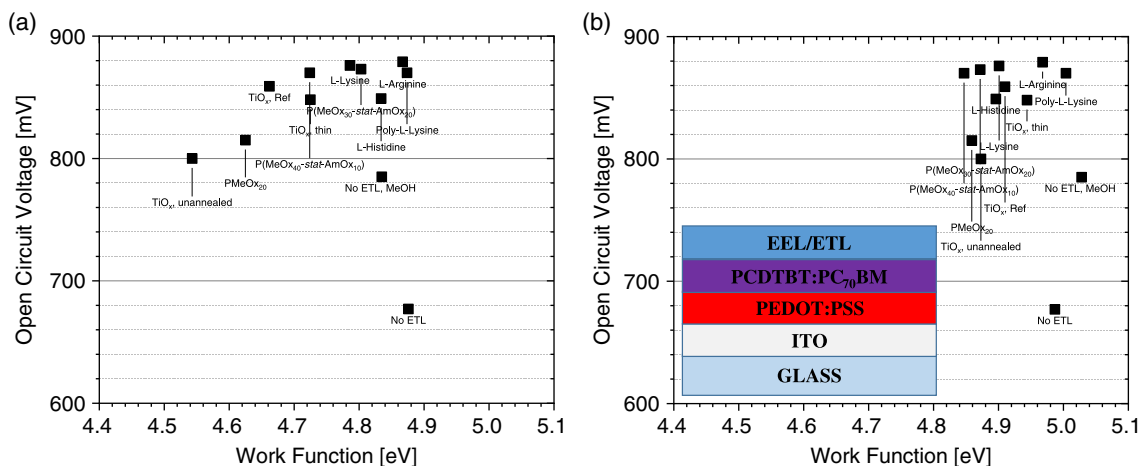


Figure 5. WF over open circuit voltage in a) dark and b) under illumination. Inset in (b) is the layer stack on which the WF was measured.

about 1 sun, yielding WF values that can be seen in the following schemes (Figure 5a,b). Intriguingly, the results displayed—if any at all—rather show an anticorrelation between the WF and the open-circuit voltage. In case of the nonilluminated layer stacks, increasing WFs do roughly correspond to increased photovoltages (Figure 5a); this seems at first glance contradictory; however, if we assume that WF changes are a result of interfacial

dipoles, which face with their positively charged part downward to the photoactive layer (and thus do attract electrons from within), the negatively charged part should face up to the outside or upper side of the layer stack. The latter situation is known for PEDOT:PSS to result in higher WFs too; however, the photoactive layer would then be processed on top of the PEDOT:PSS, enabling hole extraction, whereas in our case the photoactive

layer is buried below the CEL yielding an extraction for the opposite sign of charge—i.e., electrons. In addition, once the layer stack is illuminated, most of the applied EELs yield a WF at the upper end (compare with Figure 5b) of the values found for the dark case, thus confirming that rather high WFs measured on top of the layer stack are in correspondence of electron accumulation below the dipolar EEL. In addition, it should be considered here that the application of a metal electrode deposited from the gas phase (physical vapor deposition [PVD]) may result in a different electronic environment, and then the abrupt termination by the molecular dipoles of the EELs: the negative charge facing toward the metal may be well compensated for by the high electron density of the metal itself. Apart from these considerations of dipolar effects on charge extraction, there are several reports^[19] indicating the positive impact of CTLs

on reducing surface recombination at the electrode. The pK -value is also an indication for the readiness of the respective nitrogen of the different amine/imine groups to share one of its free electron pairs in a coordinative bond, or in other words, the pK indicates the strength of the Lewis basicity. As a consequence, an amine/imine group with a higher pK may more easily passivate defects at the interface between active layer and electrode, and therefore yield reduced surface recombination. This is also in good agreement with the trend seen for the polyoxazolines, as there is a direct proportionality between the open-circuit voltage and the amine content of these polymers, specifically.

Apart from the performance, the stability of organic solar cells is a decisive parameter for their applicability. Therefore, we studied the stability for accelerated aging under ISOS-L1 conditions using LED illumination without UV contents.^[20]

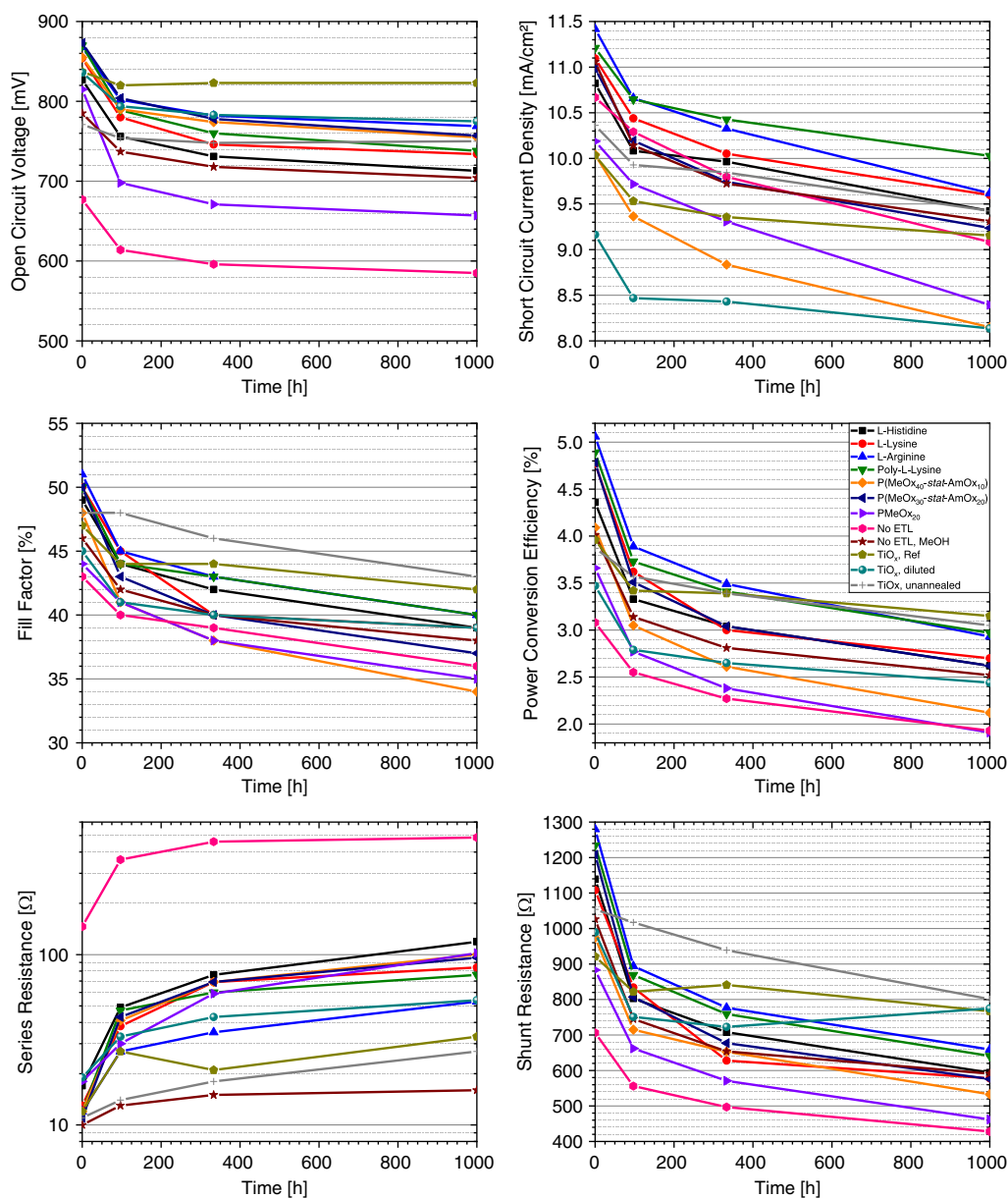


Figure 6. Aging curves for the best performing devices.

In Figure 6, the aging curves for the most stable devices for each EEL are shown. The decay curves generally follow a biexponential decay dynamic with a fast-initial decay, generally characterized as the burn-in and followed by a much slower decay. In Figure 6, the aging curves for all solar cell parameters for the longest living solar cells can be seen. For the open-circuit voltage, it can be seen that thicker TiO_x ETLs show no or a negligible burn-in, the thin TiO_x layer shows some burn-in, and all of the organic EELs reveal a clear burn-in. Interestingly, that burn-in was even stronger for L-lysine, poly-L-lysine, and P(MeOx)₂₀ than for no interfacial layer. The simple overcast of the active layer with methanol considerably reduces the burn-in depth, whereas the long-term decay proceeds with a similar rate than the solar cell without overcast. The long-term decay rate of the thin TiO_x layer is similar to the solar cell without any interlayer, suggesting a similar interface and thereby only partial coverage or diffusion of Al toward the PAL through pinholes in the TiO_x layer.

The lifetime data of the devices are shown in Table 2. From the aging data shown in Figure 6 and in Figure 31–42, Supporting Information, the burn-in time was estimated to be around 100 h; we then calculated the lifetime from the slope of between 333 and 1000 h. The lifetime energy yield (LEY)^[20b] for these devices was also determined, which is also shown in Table 2. For the amino acids EELs, there is some quite clear trend, which shows a reduction of lifetime with increasing pK_A. Poly-L-lysine has a similar lifetime and LEY to L-lysine, whereas for the polyoxazolines there is no clear trend with additional amine content. For the devices, without a transport layer the overcast with methanol alone results in an increase in the LEY by roughly 50%, which is quite a remarkable improvement. Solar cells with TiO_x as ETL show a reduction of lifetime and LEY upon thinning out the TiO_x layer

Table 2. Lifetime data of the solar cells aged under ISOS-L1 conditions. Some devices show a large standard deviation as there occurred ingress of oxygen and moisture, which accelerated degradation for individual cells.

ETL/EEL	Burn-in time [h]	Lifetime, $t_{5,80}$ [h]	Standard deviation [h]	LEY [kWh m ⁻²]	Standard deviation [kWh m ⁻²]
L-Histidine	≈100	1966	847	59.8	34.7
L-Lysine	≈100	1614	614	49.6	17.6
L-Arginine	≈100	1187	162	38.5	6.7
Poly-L-lysine	≈100	1434	188	45.8	4.9
P(MeOx ₄₀ -stat-AmOx ₁₀)	≈100	1084	184	25.7	5.9
P(MeOx ₃₀ -stat-AmOx ₂₀)	≈100	1546	270	45.3	6.5
PMeOx ₂₀	≈100	1409	291	36.4	8.5
No EEL	≈100	1347	257	29.4	5.2
Methanol overcast on PAL (no EEL)	≈100	1542	284	42.8	8.4
TiO _x , reference	≈100	2703	1235	81.9	31.1
TiO _x , diluted	≈100	1812	434	44.6	9.8
TiO _x , unannealed	≈100	1226	398	39.4	12.6

as well as without annealing of the TiO_x layer. It can be expected that for a thinned out layer there should be more pinholes in that layer and a less complete interface between metal electrode and active layer, which seems to effect lifetime negatively. For the nonannealed device, condensation and densification are to be less sufficient than for the annealed TiO_x, resulting in a more permeable interface layer, with also a higher content of remaining organic residues.

3. Conclusion

In this work, we have presented a wide variety of organic inter-layer materials that work sufficiently well as EEL. It was possible to obtain an improved understanding of their structure–property relationships. Following insights were gained based on this study: with increasing pK of the second amine group of amino acids, organic solar cell performance improved, which could be either due to dipolar effects at the interface between photoactive layer and metal electrode or tied to a reduction in surface recombination, originating from an interplay of their different functional proton donating/electron pair accepting and proton accepting/electron pair donating groups. For the subgroup of polyoxazolines, an increase in performance with an increasing content of amine groups was found. While exceptionally high stabilities remain an exclusive domain for optimally processed titanium oxides, the amino acid L-lysine resulted in a comparable stability to the metal oxide-based ETLs in this study and thereby presents an attractive, cheap, easy-processable, biocompatible, and biodegradable alternative to these.

4. Experimental Section

Polyoxazoline Preparation: 5-Aminovaleric (Alfa Aesar), acetic acid (Sigma-Aldrich), and triethylamine (Sigma-Aldrich) were used as purchased. Acetonitrile was obtained from a solvent purification system (SPS; Pure solv EN, InnovativeTechnology) and stored under argon. Methyloxazoline (Sigma-Aldrich) was dried over barium oxide (ACROS) overnight, distilled to dryness, and stored under argon (or “inert conditions”). Methyltosylate (Sigma-Aldrich) was stirred over calcium hydride (Sigma-Aldrich) overnight at 27 °C, distilled to dryness, and stored under argon. All other chemicals were obtained from commercial sources and used without further purification unless otherwise noticed. The synthesis of 2-(4-((*tert*-butoxycarbonyl)amino)butyl)-2-oxazoline (BocOx), the copolymerization of BocOx and MeOx as well as the deprotection of the polymer were done as reported in the literature with slight modification (endcapping with acetic acid and triethylamine instead of sodium azide).^[21]

Solution Preparation for EELs and ETLs: L-Histidine, L-lysine, L-arginine, P(MeOx)₂₀, P(MeOx₄₀-stat-AmOx₁₀), and P(MeOx₃₀-stat-AmOx₂₀) were dissolved in methanol at a concentration of 0.5 mg mL⁻¹ and 0.25 vol% of acetic acid was added.^[4c] Poly-L-lysine was used as a solution of 1 wt% in deionized water, which was diluted by the same volume of methanol to achieve a concentration of 0.5 wt% in a solvent ratio of water:methanol 1:1 to these solutions also 0.25 vol% of acetic acid was added. TiO_x was processed as previously reported,^[3d,22] only in the case of the diluted TiO_x, the precursor solution was diluted to 1/10 of the usual concentration by dilution with isopropanol.

Solution Preparation for Active Layer: PCDTBT (1 M) and PC₇₁BM (Solenne) were dissolved in a solvent mixture of CB:CF ratio 1:1. The concentration of PCDTBT was 5 mg mL⁻¹ and the ratio of PCDTBT to PCBM was 1:2. The solution was stirred for 2 weeks at 50 °C at 700 rpm.

Processing: Prestructured substrates of ITO on glass (Xinyan Technology Ltd., 10 Ohm sq⁻¹) were cleaned by ultrasonication for

15 min in toluene, followed by sonication for 15 min in isopropanol. Before coating, each substrate was individually dried with an air gun using dry N₂. Afterward PEDOT:PSS (Clevios PH) was spin-cast at 3000 rpm for 35 s and structured with a moist cotton tip; then they were transferred on a hot plate at 50 °C. All PEDOT:PSS samples were then annealed at 178 °C for 15 min and immediately after annealing transferred to a nitrogen glove box. PCDTBT-PC₇₁BM was spin-cast on the PEDOT:PSS at 1200 rpm for 45 s. Afterward the different EELs and ETLs were processed. For the organic EELs, multiple spin frequencies were used to vary the thickness. The chosen spin frequencies were 800, 1000, 1500, 2500, and 4000 rpm. The organic EEL solutions were spin-cast as prepared at the aforementioned spin frequencies. For the solar cells with the methanol, overcast 1 mL of methanol was dropped on the active layer, followed by spinning at 3000 rpm for 30 s to remove the Methanol. The TiO_x layers were processed according to the same procedure as earlier reported;^[3d] only in the cast of the nonannealed samples, no annealing was performed after deposition. Following the samples were placed into a mask and aluminum was evaporated at a pressure of below 5E–5 mbar. After deposition of the electrode, the size of the solar cells was determined by the overlap of patterned top and bottom electrode and resulted in 0.42 cm² devices; the solar cells were sealed with glass slides using a UV curable epoxy glue.

Characterization: Samples were characterized under a LED solar simulator (Wavelabs Sinus 70) calibrated to 1 sun intensity and with an AM1.5G spectrum. The solar cells were measured from –2 to 2 V with a NPLC of 1, a wait time of 10 ms, and a step size of 10 mV. External quantum efficiency (EQE) was characterized using a BENTHAM PVE300. The EQE was measured in a range from 300 to 900 nm in 10 nm steps; this measurement was performed without and with a light bias. To investigate the WF of different CELs, a single-point Kelvin probe system from Anfatec Instruments AG was used. All the measurements were performed in ambient air. Highly oriented pyrolytic graphite (HOPG–WF = 4.46 eV) which is chemically stable in the ambient atmosphere was used for the calibration of the Kelvin probe system. The measurements were carried out at 22 °C and 20–30% relative humidity conditions.

Degradation: Degradation experiments were performed on a self-built aging setup. The light source was white light LEDs and the temperature in the setup was set to 45 °C with the temperature sensor being shaded. The conditions were kept in accordance to ISOS-L1 protocol. Light intensity of the LED was set to an excitation density of 1 sun for these cells.

Supporting Information

Supporting Information is available from the Wiley Online Library or from the author.

Acknowledgments

Open access funding enabled and organized by Projekt DEAL.

Conflict of Interest

The authors declare no conflict of interest.

Keywords

organic charge extraction layers, organic solar cells, stability, structure-property-relationships

Received: January 31, 2020

Revised: July 8, 2020

Published online: August 12, 2020

- [1] a) Y. Cui, H. Yao, J. Zhang, T. Zhang, Y. Wang, L. Hong, K. Xian, B. Xu, S. Zhang, J. Peng, Z. Wei, F. Gao, J. Hou, *Nat. Commun.* **2019**, *10*, 2515; b) Y. Lin, B. Adilbekova, Y. Firdaus, E. Yengel, H. Faber, M. Sajjad, X. Zheng, E. Yarali, A. Seitkhan, O. M. Bakr, A. El-Labban, U. Schwingenschlögl, V. Tung, I. McCulloch, F. Laquai, T. D. Anthopoulos, *Adv. Mater.* **2019**, *31*, 1902965; c) J. Yuan, Y. Zhang, L. Zhou, G. Zhang, H.-L. Yip, T.-K. Lau, X. Lu, C. Zhu, H. Peng, P. A. Johnson, M. Leclerc, Y. Cao, J. Ulanski, Y. Li, Y. Zou, *Joule* **2019**, *3*, 1140; d) Q. Liu, Y. Jiang, K. Jin, J. Qin, J. Xu, W. Li, J. Xiong, J. Liu, Z. Xiao, K. Sun, S. Yang, X. Zhang, L. Ding, *Sci. Bull.* **2020**, *65*, 272.
- [2] a) H. Hoppe, N. S. Sariciftci, *J. Mater. Res.* **2004**, *19*, 1924; b) T. Kirchartz, P. Kaienburg, D. Baran, *J. Phys. Chem. C* **2018**, *122*, 5829.
- [3] a) W. C. H. Choy, D. Zhang, *Small* **2016**, *12*, 416; b) G. Teran-Escobar, J. Pampel, J. M. Caicedo, M. Lira-Cantu, *Energy Environ. Sci.* **2013**, *6*, 3088; c) Z. Huai, L. Wang, Y. Sun, R. Fan, S. Huang, X. Zhao, X. Li, G. Fu, S. Yang, *ACS Appl. Mater. Interfaces* **2018**, *10*, 5682; d) R. Roesch, K.-R. Eberhardt, S. Engmann, G. Gobsch, H. Hoppe, *Sol. Energy Mater. Sol. Cells* **2013**, *117*, 59; e) Z. Yin, J. Wei, Q. Zheng, *Adv. Sci.* **2016**, *3*, 1500362; f) A. G. Suren, H. Ilona Maria, B. Eva, C. Michael, H. Markus, R. S. Roar, B. Gisele Alves dos Reis, J. Mikkil, C. K. Frederik, *J. Phys. D: Appl. Phys.* **2017**, *50*, 103001; g) R. Meitzner, T. Faber, S. Alam, A. Amand, R. Roesch, M. Büttner, F. Herrmann-Westendorf, M. Presselt, L. Ciannaruchi, I. Visoly-Fisher, S. Veenstra, A. Diaz de Zerio, X. Xu, E. Wang, C. Müller, P. Troshin, M. D. Hager, S. Köhn, M. Duszka, M. Krassas, S. Züfle, E. Kymakis, E. A. Katz, S. Berson, F. Granek, M. Manceau, F. Brunetti, G. Polino, U. S. Schubert, M. Lira-Cantu, et al. *Sol. Energy Mater. Sol. Cells* **2019**, *202*, 110151.
- [4] a) Y. Zhou, C. Fuentes-Hernandez, J. Shim, J. Meyer, A. J. Giordano, H. Li, P. Winget, T. Papadopoulos, H. Cheun, J. Kim, M. Fenoll, A. Dindar, W. Haske, E. Najafabadi, T. M. Khan, H. Sojoudi, S. Barlow, S. Graham, J.-L. Brédas, S. R. Marder, A. Kahn, B. Kippelen, *Science* **2012**, *336*, 327; b) F. A. Larrain, C. Fuentes-Hernandez, W.-F. Chou, V. A. Rodriguez-Toro, T.-Y. Huang, M. F. Toney, B. Kippelen, *Energy Environ. Sci.* **2018**, *11*, 2216; c) Z. Zheng, R. Wang, H. Yao, S. Xie, Y. Zhang, J. Hou, H. Zhou, Z. Tang, *Nano Energy* **2018**, *50*, 169; d) B. Yang, S. Zhang, S. Li, H. Yao, W. Li, J. Hou, *Adv. Mater.* **2018**, *31*, 1804657; e) D. Bilby, B. Frieberg, S. Kramadhati, P. Green, J. Kim, *ACS Appl. Mater. Interfaces* **2014**, *6*, 14964.
- [5] a) G. M. Kim, I. S. Oh, A. N. Lee, S. Y. Oh, *J. Mater. Chem. A* **2014**, *2*, 10131; b) L. Yan, Y. Song, Y. Zhou, B. Song, Y. Li, *Org. Electron.* **2015**, *17*, 94; c) X. Min, F. Jiang, F. Qin, Z. Li, J. Tong, S. Xiong, W. Meng, Y. Zhou, *ACS Appl. Mater. Interfaces* **2014**, *6*, 22628; d) B. A. E. Courtright, S. A. Jenekhe, *ACS Appl. Mater. Interfaces* **2015**, *7*, 26167.
- [6] A. Li, R. Nie, X. Deng, H. Wei, S. Zheng, Y. Li, J. Tang, K.-Y. Wong, *Appl. Phys. Lett.* **2014**, *104*, 123303.
- [7] X. Zhu, B. Guo, J. Fang, T. Zhai, Y. Wang, G. Li, J. Zhang, Z. Wei, S. Duhm, X. Guo, M. Zhang, Y. Li, *Org. Electron.* **2019**, *70*, 25.
- [8] a) Y. Hirose, C. I. Wu, V. Aristov, P. Soukiassian, A. Kahn, *Appl. Surface Sci.* **1997**, *113–114*, 291; b) M. A. Baldo, S. R. Forrest, *Phys. Rev. B* **2001**, *64*, 085201; c) B. N. Limketkai, M. A. Baldo, *Phys. Rev. B* **2005**, *71*, 085207.
- [9] U. Würfel, L. Perdigón-Toro, J. Kurpiers, C. M. Wolff, P. Caprioglio, J. J. Rech, J. Zhu, X. Zhan, W. You, S. Shoaee, D. Neher, M. Stollerfoht, *J. Phys. Chem. Lett.* **2019**, *10*, 3473.
- [10] T. Kirchartz, B. E. Pieters, K. Taretto, U. Rau, *Phys. Rev. B* **2009**, *80*, 035334.
- [11] Z. Hu, Z. Zhong, K. Zhang, Z. Hu, C. Song, F. Huang, J. Peng, J. Wang, Y. Cao, *NPG Asia Mater.* **2017**, *9*, e379.
- [12] J. Kim, A. Ho-Baillie, S. Huang, *Sol. RRL* **2019**, *3*, 1800302.

- [13] R. Roesch, M. Seeland, M. Baerenklau, G. Gobsch, H. Hoppe, *Sol. Energy Mater. Sol. Cells* **2013**, *111*, 212.
- [14] S. Beaupré, M. Leclerc, *J. Mater. Chem. A* **2013**, *1*, 11097.
- [15] a) C. H. Peters, I. T. Sachs-Quintana, J. P. Kastrop, S. Beaupré, M. Leclerc, M. D. McGehee, *Adv. Energy Mater.* **2011**, *1*, 491; b) W. R. Mateker, I. T. Sachs-Quintana, G. F. Burkhard, R. Cheacharoen, M. D. McGehee, *Chem. Mater.* **2015**, *27*, 404.
- [16] L. Ye, H. Hu, M. Ghasemi, T. Wang, B. A. Collins, J.-H. Kim, K. Jiang, J. H. Carpenter, H. Li, Z. Li, T. McAfee, J. Zhao, X. Chen, J. L. Y. Lai, T. Ma, J.-L. Bredas, H. Yan, H. Ade, *Nat. Mater.* **2018**, *17*, 253.
- [17] A. Wagenpfahl, D. Rauh, M. Binder, C. Deibel, V. Dyakonov, *Phys. Rev. B* **2010**, *82*, 115306.
- [18] a) L. Ye, Y. Jing, X. Guo, H. Sun, S. Zhang, M. Zhang, L. Huo, J. Hou, *J. Phys. Chem. C* **2013**, *117*, 14920; b) H. Zhou, Y. Zhang, J. Seifert, S. D. Collins, C. Luo, G. C. Bazan, T.-Q. Nguyen, A. J. Heeger, *Adv. Mater.* **2013**, *25*, 1646; c) S. Guo, B. Cao, W. Wang, J.-F. Moulin, P. Müller-Buschbaum, *ACS Appl. Mater. Interfaces* **2015**, *7*, 4641.
- [19] a) K. M. Knesting, H. Ju, C. W. Schlenker, A. J. Giordano, A. Garcia, O. N. L. Smith, D. C. Olson, S. R. Marder, D. S. Ginger, *J. Phys. Chem. Lett.* **2013**, *4*, 4038; b) J. Reinhardt, M. Grein, C. Bühler, M. Schubert, U. Würfel, *Adv. Energy Mater.* **2014**, *4*, 1400081; c) S. Wheeler, F. Deledalle, N. Tokmoldin, T. Kirchartz, J. Nelson, J. R. Durrant, *Phys. Rev. Appl.* **2015**, *4*, 024020.
- [20] a) M. O. Reese, S. A. Gevorgyan, M. Jorgensen, E. Bundgaard, S. R. Kurtz, D. S. Ginley, D. C. Olson, M. T. Lloyd, P. Moryllo, E. A. Katz, A. Elschner, O. Hailliant, T. R. Currier, V. Shrotriya, M. Hermenau, M. Riede, K. R. Kirov, G. Trimmel, T. Rath, O. Inganas, F. L. Zhang, M. Andersson, K. Tvingstedt, M. Lira-Cantu, D. Laird, C. McGuinness, S. Gowrisanker, M. Pannone, M. Xiao, J. Hauch, et al., *Sol. Energy Mater. Sol. Cells* **2011**, *95*, 1253; b) R. Roesch, T. Faber, E. von Hauff, T. M. Brown, M. Lira-Cantu, H. Hoppe, *Adv. Energy Mater.* **2015**, *5*, 24; c) E. A. K. Mark, V. Khenkin, A. Abate, G. Bardizza, J. J. Berry, C. J. Brabec, F. Brunetti, V. Bulović, Q. Burlingame, A. Di Carlo, R. Cheacharoen, Y.-B. Cheng, A. Colsmann, S. Cros, K. Domanski, M. Dusza, C. J. Fell, S. R. Forrest, Y. Galagan, D. Di Girolamo, M. Grätzel, A. Hagfeldt, E. von Hauff, H. Hoppe, J. Kettle, H. Köbler, M. S. Leite, S. Liu, Y.-L. Loo, J. M. Luther, et al., *Nat. Energy* **2020**, *5*, 35; d) M. V. Khenkin, E. A. Katz, A. Abate, G. Bardizza, J. J. Berry, C. Brabec, F. Brunetti, V. Bulović, Q. Burlingame, A. Di Carlo, R. Cheacharoen, Y.-B. Cheng, A. Colsmann, S. Cros, K. Domanski, M. Dusza, C. J. Fell, S. R. Forrest, Y. Galagan, D. Di Girolamo, M. Grätzel, A. Hagfeldt, E. von Hauff, H. Hoppe, J. Kettle, H. Köbler, M. S. Leite, S. Liu, Y.-L. Loo, J. M. Luther, et al., *Nat. Energy* **2020**, *5*, 35.
- [21] a) M. Hartlieb, D. Pretzel, K. Kempe, C. Fritzsche, R. M. Paulus, M. Gottschaldt, U. S. Schubert, *Soft Matter* **2013**, *9*, 4693; b) T. Lühmann, M. Schmidt, M. N. Leiske, V. Spieler, T. C. Majdanski, M. Grube, M. Hartlieb, I. Nischang, S. Schubert, U. S. Schubert, L. Meinel, *ACS Biomater. Sci. Eng.* **2017**, *3*, 304.
- [22] J. Y. Kim, S. H. Kim, H.-H. Lee, K. Lee, W. Ma, X. Gong, A. J. Heeger, *Adv. Mater.* **2006**, *18*, 572.